

## Article

# Design and Optimization of an Ultraviolet Scattering Communication System Based on Duty Cycle Regulation

Yu Jiao <sup>1,2,†</sup>, Yingkai Zhao <sup>1,2,†</sup> , Li Kuang <sup>1,3</sup>, Ranxi Lin <sup>1,2</sup>, Jin Ning <sup>1,\*</sup> and Jianguo Liu <sup>1,2,\*</sup>

- <sup>1</sup> Laboratory of Nano Optoelectronics, Institute of Semiconductors, Chinese Academy of Sciences, Beijing 100083, China; jiaoyu@semi.ac.cn (Y.J.); zhaoyingkai20@semi.ac.cn (Y.Z.); kuangli@semi.ac.cn (L.K.); linranxi99@semi.ac.cn (R.L.)
- <sup>2</sup> School of Electronic, Electrical and Communication Engineering, University of Chinese Academy of Sciences, Beijing 100049, China
- <sup>3</sup> College of Materials Science and Opto-Electronic Technology, University of Chinese Academy of Sciences, Beijing 100049, China
- \* Correspondence: ningjin@semi.ac.cn (J.N.); jgliu@semi.ac.cn (J.L.)
- † These authors contributed equally to this work.

**Abstract:** In this paper, a novel ultraviolet (UV) scatter communication scheme is presented, designed to dynamically adjust the signal duty cycle to optimize on–off keying (OOK) modulation and reduce the bit error rate (BER), particularly under varying rate settings. This approach addresses the significant challenge posed by LED tailing effects, which cause signal fluctuations and increase BER in high-speed communications. This BER suppression scheme is proposed for the first time in UV communication research, enhancing communication performance without the need for additional hardware or complex algorithms. A UV communication model that incorporates both path loss and LED tailing effects is introduced, with the probability density function of the signal from transmitter to receiver derived. By varying the signal duty cycle, tailing-induced BER is effectively minimized. Additionally, a closed-form expression for signal transmission BER using a single-scattering model is provided, and the proposed UV communication system is validated through comprehensive simulations and experimental tests. The results indicate that LED tailing has a pronounced impact on BER at higher communication speeds, while its effects are less significant at lower speeds. By optimizing the duty cycle parameters for various communication rates, findings demonstrate that lower duty cycle settings significantly reduce the BER at higher speeds. This further demonstrates the excellent performance of the proposed UV communication solution for OOK-modulated optical communication.



**Citation:** Jiao, Y.; Zhao, Y.; Kuang, L.; Lin, R.; Ning, J.; Liu, J. Design and Optimization of an Ultraviolet Scattering Communication System Based on Duty Cycle Regulation.

*Photonics* **2024**, *11*, 662. <https://doi.org/10.3390/photonics11070662>

Received: 7 June 2024  
Revised: 12 July 2024  
Accepted: 14 July 2024  
Published: 16 July 2024



**Copyright:** © 2024 by the authors. Licensee MDPI, Basel, Switzerland. This article is an open access article distributed under the terms and conditions of the Creative Commons Attribution (CC BY) license (<https://creativecommons.org/licenses/by/4.0/>).

**Keywords:** UV scattering communication; signal duty cycle; LED tailing

## 1. Introduction

UV wireless optical communication is a technology that utilizes UV light sources for data transmission and communication in the atmosphere [1]. This method is based on the unique properties of UV light to transmit information through the atmosphere and is typically used for short-range, high-speed communication, serving as an important supplement to conventional communication methods. UV light communication has received widespread attention due to its advantages in non-line-of-sight communication, strong interference resistance, and low environmental noise. Solar UV radiation in the UV spectrum is heavily absorbed by ozone molecules as it traverses the atmosphere, resulting in nearly zero UV radiation intensity reaching the Earth's surface. This creates conditions of extremely low environmental light noise conducive to UV light communication [2]. Compared to visible light, UV light has a shorter wavelength and stronger scattering ability, providing advantages for non-line-of-sight scatter communication [3–5]. Additionally, UV light communication offers benefits in interference resistance and confidentiality [6],

enabling it to provide stable and efficient communication capabilities in complex and specialized communication environments [7].

The development of UV wireless communication systems involves advancements in scattering channel models to describe UV signal propagation characteristics in various environments. These models are critical for optimizing UV communication system performance, particularly in non-line-of-sight (NLOS) scenarios where direct signal transmission is hindered. Most UV scattering channel models use stochastic geometric frameworks and Monte Carlo methods to simulate and calculate link gains [8–10]. UV NLOS scattering communication primarily estimates path loss in NLOS channels using single-scattering models [8]. Initially proposed for detailed analysis of UV scattering channel properties, single-scattering models have been subject to recent experimental studies on short-range NLOS scattering channels [11,12]. Single-scattering and Monte Carlo-based multi-scattering models have been developed by researchers to study the effects of atmospheric turbulence, investigating parameters such as pulse effects, path loss, and bandwidth, while also conducting simulation studies on the impact of transmitter and receiver elevation angles on system error rates [8]. Additionally, a non-Monte Carlo-based NLOS UV communication system channel model has been proposed, focusing solely on single-scattering and double-scattering events. This model, compared to Monte Carlo-based approaches, demonstrates superior communication performance [13].

The use of UV LEDs for UV NLOS scattering communication in ultraviolet communication systems has been widely studied [14–16]. Published experiments have shown that data transmission rates of up to 2 kbps can be achieved at distances of 100 m [17]. A multiple input multiple output (MIMO) UV communication system has been successfully designed, enabling stable communication distances of 30 m with a data transmission rate of 250 kbps while maintaining an acceptable error rate [18]. Additionally, an outdoor NLOS UV communication platform has been established, enabling outdoor communication distances of up to 500 m with a data rate of 400 kbps and a frame error rate of  $10^{-5}$  [19]. However, the tailing effect of UV LED emissions can degrade the quality of UV communication, leading to an increase in BER. In this context, our study focuses on investigating the impact of LED tailing on system BER and evaluates the performance of UV communication systems when adjusting the signal duty cycle to mitigate the effects of tailing. We employ 265 nm LEDs to transmit UV signals using OOK modulation. A photomultiplier tube (PMT) serves as the system receiver, with PMT output data sampled and processed through operational amplifier circuits and ADC chips before being transmitted to a data processing module composed of FPGA chips and peripheral circuits. In this module, a signal processing algorithm based on discrete Poisson distribution channel models and signal correlation detection is used for decoding optical pulse signal data. The theoretical analysis explores the relationship between ideal scenarios, tailing effects, and varying signal duty cycles in relation to system BER. Subsequently, system performance is evaluated through computer simulations, FPGA-based hardware systems are developed to implement UV communication, the impact of duty cycle changes on system BER is tested, and the effectiveness of our approach is validated through real-time outdoor communication experiments. Through derivations, the relationship between different duty cycles and BER under the influence of tailing effects is established. Furthermore, an analysis is conducted on how changes in transmission rate and distance affect BER when altering the signal duty cycle. By elucidating these relationships, insights are provided for optimizing UV communication systems operating under the influence of LED tailing effects, and guidance is offered for improving BER in UV communication systems employing OOK modulation.

In Section 2, scattering models and discrete Poisson distribution are analyzed, and formulas for theoretical states, LED tailing effects, and BER under varying duty cycle conditions are derived. Section 3 employs computer simulations to examine the relationship between ideal scenarios, tailing effects, and varying signal duty cycles with respect to system BER. In Section 4, outdoor experiments were conducted, and the experimental results were discussed. Section 5 provides a comprehensive summary of the entire paper.

## 2. Theoretical Formula Derivation

### 2.1. Single-Scattering Channel Model

The communication system we discuss is established based on a coplanar single-scattering model, which forms the foundation for analyzing the transmission–channel–reception communication link. Figure 1 illustrates the diagram of a UV NLOS scattering communication link in coplanar geometry, where the transmitter (Tx) is located at point T and the receiver (Rx) is at point R. The defined parameters are as follows:  $\theta_1$  and  $\theta_2$  are the angles between the communication devices and the horizontal axis at Tx and Rx, respectively;  $\phi_1$  and  $\phi_2$  are the transmitter-side beam divergence angle and receiver-side field of view (FOV) angle;  $\theta_s$  represents the scattering angle between the emission direction of the incident light and the receiving direction, satisfying  $\theta_s = \theta_1 + \theta_2$ ;  $r$  denotes the straight-line distance between the transmitter and receiver;  $r_1$  and  $r_2$ , respectively, represent the distances from the scattering center to Tx and Rx.

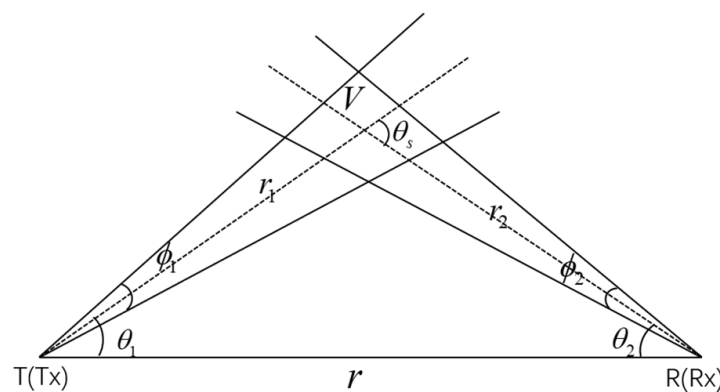


**Figure 1.** The diagram of a UV NLOS scattering communication link in coplanar geometry.

The scattered energy at Rx caused by a differential volume source [20] is calculated as follows:

$$\delta E_r = \frac{E_t k_s P(\mu) A_r \delta V \cos \zeta \exp[-k_e(r_1 + r_2)]}{\Omega_1 r_1^2 r_2^2}, \tag{1}$$

In this context,  $E_t$  represents the emitted UV light energy;  $\Omega_1$  denotes the solid angle of radiation cone from the transmitter (Tx);  $\delta V$  is the common volume intersecting the emission and reception ends;  $k_e$  is the atmospheric extinction coefficient, given by  $k_e = k_s + k_a$ , where  $k_s$  and  $k_a$  are the scattering and absorption coefficients, respectively;  $A_r$  represents the area of the receiving aperture;  $P(\mu)$  is the scattering phase function, where  $\mu = \cos \theta_s$ ; and  $\zeta$  is the angle between the Rx axis and the vector from Rx to the common volume. Based on the respective scattering coefficients, the scattering phase function is modeled as a weighted sum of Rayleigh (molecular) and Mie (aerosol) scattering phase functions [9] calculated as follows:

$$P(\mu) = \frac{k_s^{Ray}}{k_s} p^{Ray}(\mu) + \frac{k_s^{Mie}}{k_s} p^{Mie}(\mu), \tag{2}$$

Here,  $k_s^{Ray}$  and  $k_s^{Mie}$  represent the Rayleigh and Mie scattering coefficients, respectively, with  $k_s = k_s^{Ray} + k_s^{Mie}$ .  $p^{Ray}(\mu)$  and  $p^{Mie}(\mu)$  representing the Rayleigh and Mie scattering phase functions, following the generalized Rayleigh model and the generalized Henyey–Greenstein function. Subsequently, we define the path loss as  $PL = E_t/E_r$ . The path loss expression of the truncated cone approximation model is given by the following equation [9]:

$$PL \approx \frac{96r \sin \theta_1 \sin^2 \theta_2 (1 - \cos \frac{\phi_1}{2}) \exp[\frac{k_e r (\sin \theta_1 + \sin \theta_2)}{\sin \theta_s}]}{k_s P(\mu) A_r \phi_1^2 \phi_2 \sin \theta_s (12 \sin^2 \theta_2 + \phi_2^2 \sin^2 \theta_1)}, \tag{3}$$

This closed-form expression allows for the analysis and handling of path loss, as well as the BER performance of communication systems under different geometric conditions. Subsequent simulations and experiments are also based on this expression.

### 2.2. Poisson Distribution

We utilize the Poisson distribution to describe the probability distribution of receiving photons in UV light communication. The Poisson distribution expression is given by the following:

$$P(X = n) = e^{-\lambda} \frac{\lambda^n}{n!}, \lambda > 0, \tag{4}$$

Here,  $X$  represents the count of events (number of photons detected), which is a non-negative integer. The parameter  $\lambda$  represents the average number of UV photons arriving at the receiver per unit time (Poisson parameter). The probability mass function  $P(X = n)$  represents the probability of detecting exactly  $n$  photons at the receiver within a unit time interval.

For a single symbol, under OOK modulation, the mean number of photons for symbol 1 at the transmitter is  $\lambda_s$ . Therefore, the probability density function of receiving photon counts for any symbol 1 can be expressed as follows:

$$P_{one}(n) = \frac{e^{-\lambda_s} \cdot \lambda_s^n}{n!}, \tag{5}$$

Here,  $n$  represents the number of photons, and  $P_{one}(n)$  denotes the probability of receiving  $n$  photons when transmitting symbol 1. Similarly, assuming the mean number of photons for symbol 0 at the transmitter under OOK modulation is  $\lambda_b$ , the probability density function of receiving photon counts for symbol 0 can be expressed as follows:

$$P_{zero}(n) = \frac{e^{-\lambda_b} \cdot \lambda_b^n}{n!}, \tag{6}$$

Here,  $n$  represents the number of photons,  $P_{zero}(n)$  represents the probability of receiving  $n$  photons when transmitting symbol 0. We can use the above two Poisson formulas to characterize the probability of receiving photon signals by the system.

### 2.3. Derivation of Ideal BER

In this section, the formula for the system BER under ideal LED emission conditions is derived. The relationship between the emission power of an LED and its driving current can be described through the optoelectronic characteristics of the LED. These optoelectronic characteristics can be expressed by the following equation:

$$P_{LED} = I_{LED} \times U_{LED}, \tag{7}$$

Here,  $P_{LED}$  represents the emission power of the LED,  $I_{LED}$  denotes the driving current, and  $U_{LED}$  stands for the operating voltage.

The emission characteristics of LED in the ideal state are illustrated in Figure 2.

The theoretical emitted light energy for symbols 1 and 0 within a unit symbol time can be obtained with the following formula:

$$IL_{zero} \cdot T = \eta \cdot \int_{t=T}^{t=2T} I_{off}(t) V dt, \tag{8}$$

$$IL_{one} \cdot T = \eta \cdot \int_{t=0}^{t=T} I_{on}(t) V dt, \tag{9}$$

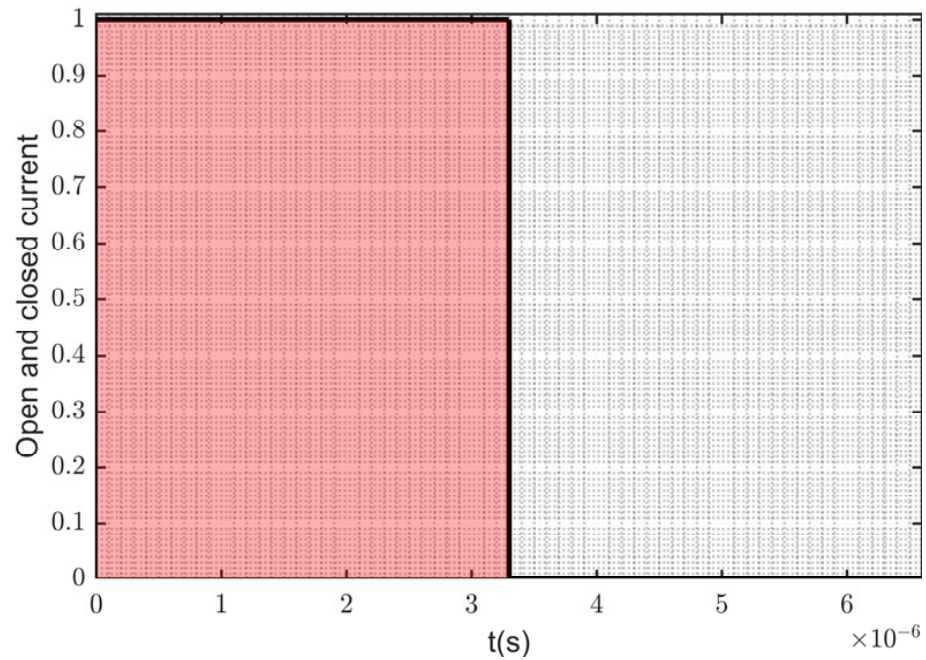


**Figure 2.** Current variation curve of an LED in ideal operation mode.

In the above formulas,  $IL$  is defined as the luminous power of the LED per unit time.  $IL \cdot T$  represents the optical energy radiated during a single symbol time. The duration of symbol emission  $T$  represents the duration of light emission for a single symbol in the system and is related to the system’s communication rate.  $\eta$  represents the electro–optical conversion efficiency of the LED,  $I(t)$  denotes the current at a given time  $t$ , and  $V$  stands for the voltage applied to the LED.

For a UV communication system, the sources of photons for symbol 0 mainly include the following three aspects: ① PMT dark count noise; ② ambient light noise; ③ LED emission tail noise. Therefore, for an ideal UV communication system, the mean expressions for the number of received photons for symbols 1 and 0 at the receiver are as follows:

$$\lambda_s = N_{dk} + N_{lt} + IL_{one} \cdot T \cdot \alpha / E_{photon}, \tag{10}$$

$$\lambda_b = N_{dk} + N_{lt} + IL_{zero} \cdot T \cdot \alpha / E_{photon}, \tag{11}$$

In the above expression,  $N_{dk}$  represents the number of photons generated by the dark current noise introduced into the communication system per symbol, and  $N_{lt}$  represents the number of photons generated by introduced light noise per symbol.  $E_{photon}$  denotes the energy of a single UV photon,  $\alpha$  represents the system attenuation coefficient.

By obtaining the values of  $\lambda_s$  and  $\lambda_b$  from the above equation, and substituting them into the Poisson distribution expression, it is possible to describe the probability of symbols 1 and 0 generating a certain number of received photons  $n$  at the receiver.

During the signal recovery process, it is necessary to determine the threshold for symbol 0/1 decision. The decision threshold is related to the Poisson distribution probability expression. The BER can then be expressed as follows:

$$BER(x_0) = \frac{1}{2} \left( \sum_{n=x_0+1}^{\infty} P_{zero}(n) \right) + \frac{1}{2} \left( 1 - \sum_{n=x_0+1}^{\infty} P_{one}(n) \right), \tag{12}$$

Here,  $x_0$  represents the 0/1 decision threshold, and  $BER(x_0)$  denotes the bit error rate performance at the  $x_0$  threshold. By calculating the above equation, the BER of the UV communication system can be obtained in the ideal scenario where there is no LED emission tailing effect.

### 2.4. Derivation of BER Considering Tailing Effects

LED point-to-point when there is a tailing effect (also known as trailing effect) is a phenomenon in LED display technology. The emission tailing noise is caused by the charging and discharging of the LED capacitor. For a typical RC circuit, the charging current function is calculated as follows:

$$I_{on}(t) = \frac{V \cdot (1 - \exp(-t/RC))}{R}, \tag{13}$$

In this context,  $R$  represents the resistance value in the circuit, and  $C$  represents the capacitance value. The discharge current function is as follows:

$$I_{off}(t) = \frac{V \cdot \exp(-t/RC)}{R}, \tag{14}$$

In conventional OOK modulation systems, symbols 0 and 1 each occupy 50% of the duty cycle. Because there is a gradual brightening phenomenon when the LED is turned on and a trailing phenomenon when it is turned off, the duration required for the LED to reach 50% brightness upon startup and to diminish to 50% brightness upon shutdown satisfies the following formula:

$$I_{on}(t_0) = I_{off}(t_0), \tag{15}$$

During the startup and shutdown of the LED, a small amount of emitted light may be erroneously counted as symbol 0, as shown in Figure 3. Such misidentification can have a detrimental impact on the BER of the entire communication system.

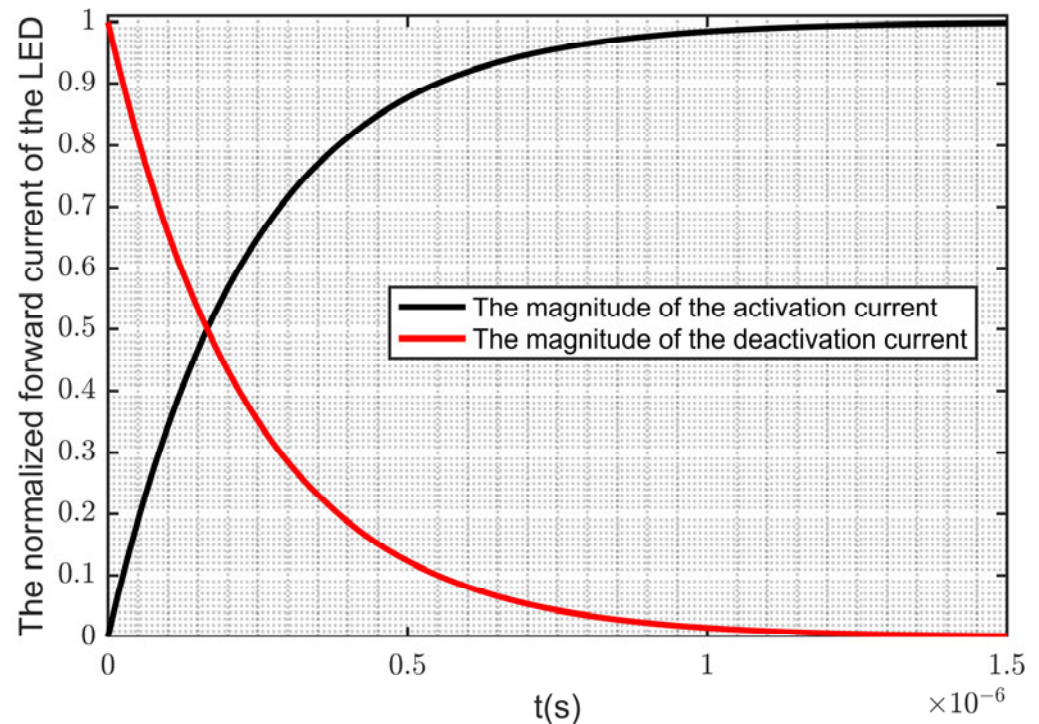


Figure 3. The current variation curve during LED charging and discharging.

In Figure 4, it can be observed that due to the presence of LED trailing effects, there is a partial rightward offset in the maximum likelihood position in ultraviolet correlation detection. At this point, the current expression transitions from the ideal state to the charging and discharging state of the RC circuit. The formula expression for LED emission energy can be obtained by calculating the energy of signal light and noise light as follows:

$$IL_{one} \cdot T = (\eta V / R) \cdot T - \eta \left( \int_{t=0}^{t=t_0} I_{on}(t) V dt \right) + \eta \left( \int_{t=t_0+T}^{t=2T} I_{off}(t) V dt \right), \quad (16)$$

$$IL_{zero} \cdot T = \eta \left( \int_{t=0}^{t=t_0} I_{on}(t) V dt \right) + \eta \left( \int_{t=t_0+T}^{t=2T} I_{off}(t) V dt \right), \quad (17)$$

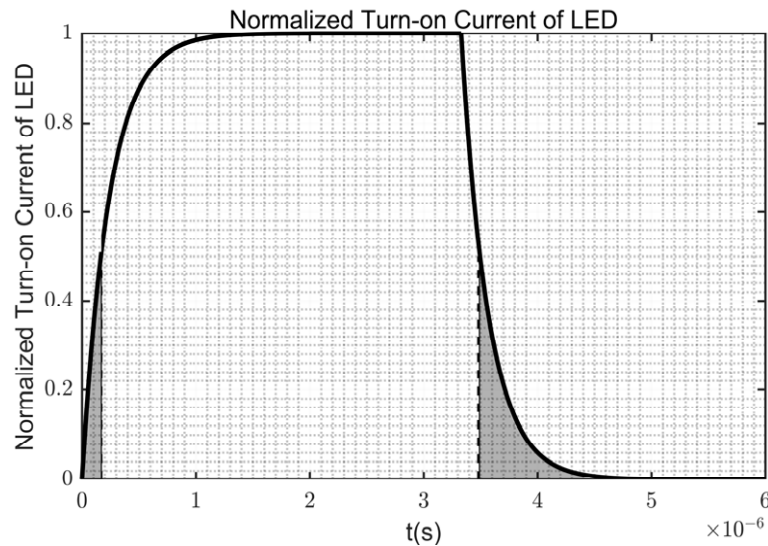


Figure 4. The current variation curve during LED emission tailing.

The ratio  $\sigma$  of this noise intensity to the signal light intensity is calculated as follows:

$$\sigma = \frac{IL_{zero} \cdot T}{IL_{one} \cdot T} = \frac{\eta \left( \int_{t=0}^{t=t_0} I_{on}(t) V dt \right) + \eta \left( \int_{t=t_0+T}^{t=2T} I_{off}(t) V dt \right)}{(\eta V / R) \cdot T - \eta \left( \int_{t=0}^{t=t_0} I_{on}(t) V dt \right) + \eta \left( \int_{t=t_0+T}^{t=2T} I_{off}(t) V dt \right)} \approx \frac{\eta \left( \int_{t=0}^{t=t_0} I_{on}(t) V dt \right) + \eta \left( \int_{t=t_0+T}^{t=2T} I_{off}(t) V dt \right)}{(\eta V / R) \cdot T}, \quad (18)$$

By substituting the expressions from Formulas (16) and (17) into Formulas (10) and (11), we determine the values of the Poisson distribution constants  $\lambda_s$  and  $\lambda_b$  considering the influence of tail effects. Introducing  $\sigma$  facilitates the simplification of Formula (11), where Formula (11) can be replaced by the conjunction of Formula (16) and  $\sigma$ . Subsequently,  $\lambda_s$  and  $\lambda_b$  are incorporated into Poisson distribution Formulas (5) and (6) to derive the Poisson distribution probability density expressions. This process culminates in deriving the BER expression as a function of the decision threshold  $x_0$  variation:

$$BER(x_0) = \frac{1}{2} \left( \sum_{n=x_0+1}^{\infty} P_{zero}(n) \right) + \frac{1}{2} \left( 1 - \sum_{n=x_0+1}^{\infty} P_{one}(n) \right), \quad (19)$$

The BER variation of the UV communication system considering the influence of LED trailing effects can be calculated using Formula (19).

### 2.5. Derivation of BER with Changes in Transmission Signal Duty Cycle

This paper proposes a scheme to mitigate the impact of trailing effects by changing the transmission signal duty cycle. The duty cycle can be calculated using the following formula:

$$D = \frac{PW}{T} \times 100\%, \quad (20)$$

where  $PW$  represents the duration of the high level of a signal,  $T$  denotes the total time of one complete period, and  $D$  represents the duty cycle of the signal.

The specific implementation of the proposed scheme is to appropriately reduce the duty cycle of LED emission, i.e., to decrease the duration of high-level emission of the ultraviolet LED chip. The untreated duty cycle of LED emission is generally 50%. Building upon OOK modulation, the duty cycle of symbol 1 can be shortened to  $\xi$ . At this stage, the formula for the LED's luminous energy per symbol unit is expressed as follows:

$$IL_{one}(\xi) \cdot T = (\eta V/R) \cdot T - \eta \left( \int_{t=0}^{t=t_\xi} I_{on}(t) V dt \right) + \eta \left( \int_{t=t_\xi+T}^{t=2T} I_{off}(t) V dt \right), \tag{21}$$

$$IL_{zero}(\xi) \cdot T = \eta \left( \int_{t=0}^{t=t_\xi} I_{on}(t) V dt \right) + \eta \left( \int_{t=t_\xi+T}^{t=2T} I_{off}(t) V dt \right), \tag{22}$$

The ratio of this noise intensity to the signal light intensity is expressed as follows:

$$\begin{aligned} \sigma(\xi) &= \frac{IL_{zero}(\xi) \cdot T}{IL_{one}(\xi) \cdot T} = \frac{\eta \left( \int_{t=0}^{t=t_\xi} I_{on}(t) V dt \right) + \eta \left( \int_{t=t_\xi+T}^{t=2T} I_{off}(t) V dt \right)}{(\eta V/R) \cdot T - \eta \left( \int_{t=0}^{t=t_\xi} I_{on}(t) V dt \right) + \eta \left( \int_{t=t_\xi+T}^{t=2T} I_{off}(t) V dt \right)} \tag{23} \\ &\approx \frac{\eta \left( \int_{t=0}^{t=t_\xi} I_{on}(t) V dt \right) + \eta \left( \int_{t=t_\xi+T}^{t=2T} I_{off}(t) V dt \right)}{(\eta V/R) \cdot T}, \end{aligned}$$

Utilizing the BER formula associated with the Poisson distribution probability formula, the variation curve of the BER when the duty cycle changes can be calculated.

By adjusting the duty cycle, it is possible to reduce the luminous intensity of symbol 0, thereby reducing the probability of misjudgment, as shown in Figure 5. However, at the same time, the luminous intensity of symbol 1 will also decrease as the duty cycle decreases. Therefore, for specific rates, there exists an optimal duty cycle selection position. Additionally, since the RC charging and discharging time is fixed, the influence of trailing effects on the BER will diminish for lower rates. In such cases, the choice of duty cycle tends to approach 50%. In other words, changing the duty cycle has a smaller impact on lower rates.

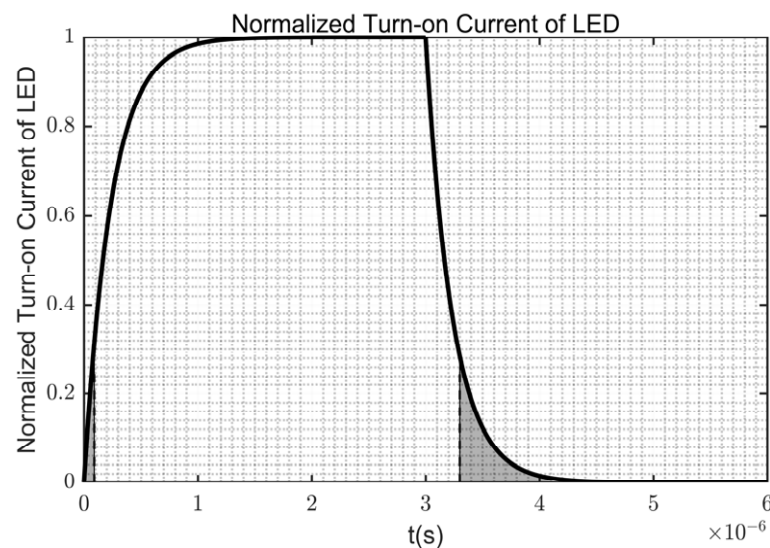


Figure 5. The conduction current variation curve of LED when the duty cycle changes.

The theoretical derivation in this section reveals that, under a specific rate, improving the duty cycle of the transmitted signal can ameliorate the degradation in BER caused by the LED’s trailing effect in UV communication, thereby enhancing communication stability and quality. In the subsequent chapters, Sections 3 and 4, we will verify and analyze this scheme through computer simulation and outdoor field hardware experiments, respectively.

### 3. Simulation Implementation

#### 3.1. Simulating the Photon States at the Transmitter, Noise, and Receiver End

In the UV scattering optical communication system under consideration, OOK modulation is employed. The simulation conditions at the transmitter end are as follows: a communication rate of 300 kbps is set, and the LED array operates with a forward voltage of 1 V. As the LEDs switch on and off, the data signal is transmitted into the atmospheric channel.

We simulated the optoelectronic characteristics of the system at different stages, as shown in the figure above. Figure 6a depicts the square wave output waveform of the signal transmission, with the LED emitting light at a high level. Figure 6b illustrates the simulated environmental noise interference. Figure 6c presents the discrete photocurrent received by the PMT. It can be observed that the occurrence frequency and amplitude of noise exhibit certain randomness. When introduced into the data signal, this noise, further amplified by the PMT and operational amplifier circuitry, can interfere with the communication quality of the system.

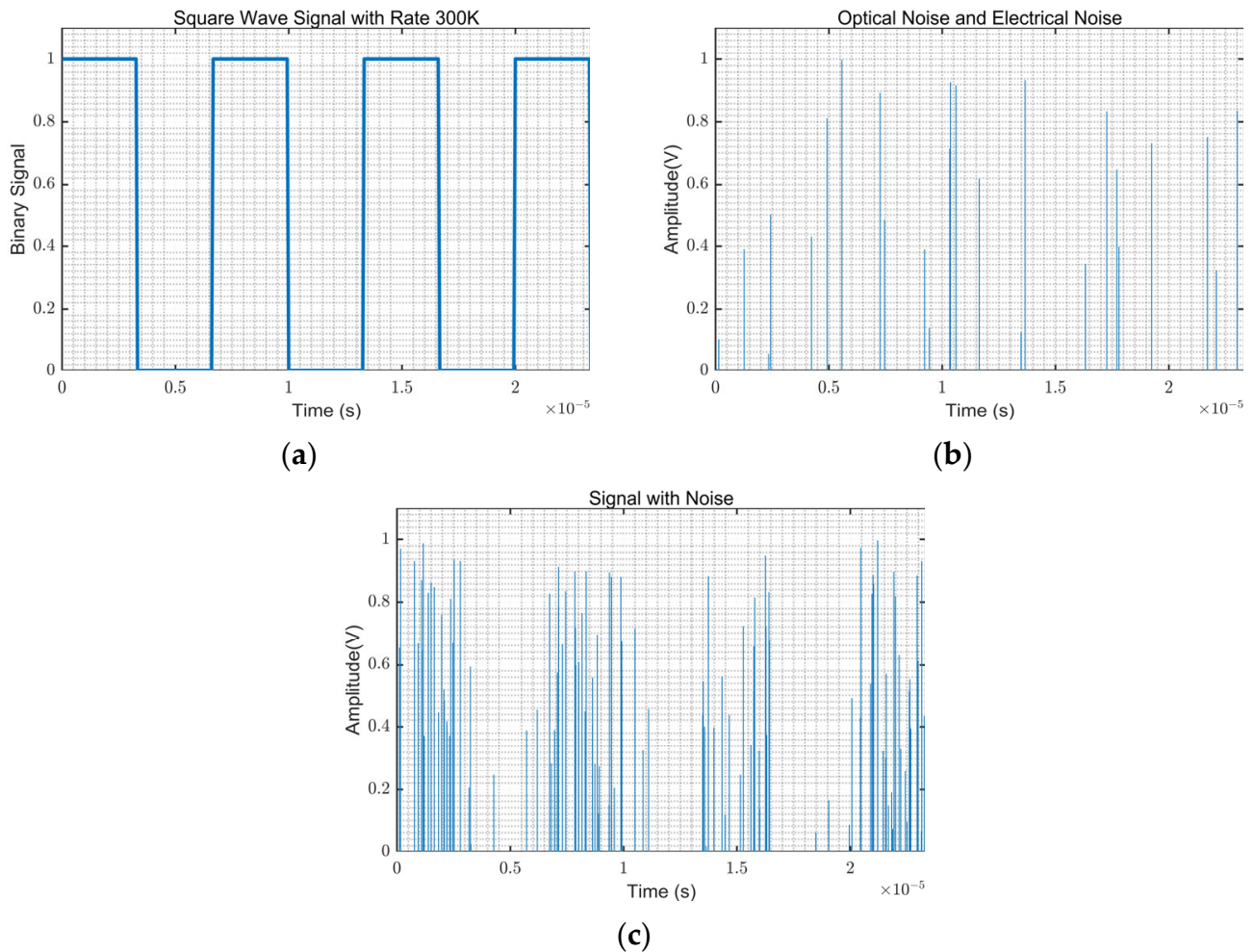


**Figure 6.** (a) Amplitude variation of the signal at the transmitting end. (b) The amplitude of introduced noise. (c) Signal amplitude at the receiving end.

### 3.2. Path Loss Simulation

In the previous section, we simulated the optoelectronic characteristics at different stages. In this section, we establish the ultraviolet communication single-scattering channel based on the scattering model formula and simulate the variation curve of path loss with increasing distance. According to the single-scattering model, we estimated the path loss for communication distances ranging from 100 m to 1000 m. The specific parameters for this simulation are as follows: the elevation angle of the transmitter and receiver is set to  $10^\circ$ , the emission angle is  $30^\circ$ , the receiver's field of view angle is  $120^\circ$ , atmospheric absorption loss  $k_a$  is  $9 \times 10^{-4}$ , scattering coefficient  $k_s$  is  $7.7 \times 10^{-4}$ , the receiving aperture  $A_r$  is  $5 \times 10^{-4}$ , the asymmetry factor  $g$  is 0.72, and  $f = 0.5$ . In Figure 7 of the simulation, it is evident that as the communication distance increases, the path loss of ultraviolet light transmission in the atmosphere also increases. This increase in path loss is measured in decibels.

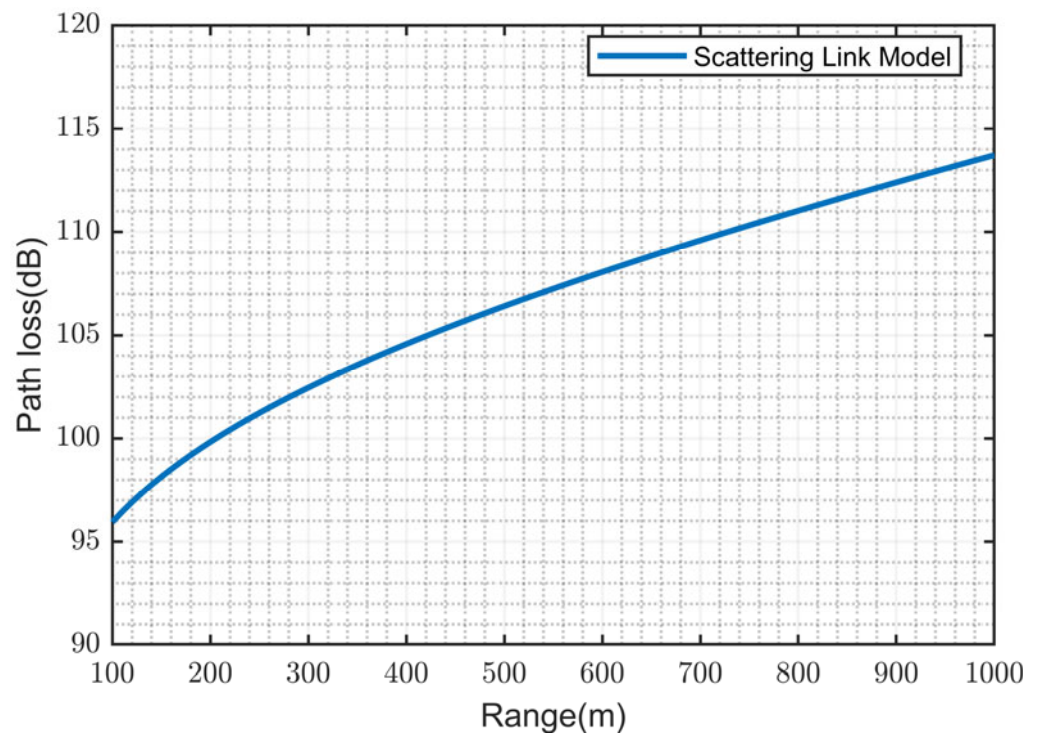


Figure 7. Path loss from approximated models.

By establishing the aforementioned path loss simulation, we have laid the foundation for subsequent simulation analyses on the relationship between parameters such as BER and distance.

### 3.3. The Impact of Decision Thresholds on BER at Different Rates

The curves of BER against the variation of decision thresholds were plotted for ideal communication rates of 300 kbps and 150 kbps. The BER formula, derived from the Poisson formula in Section 2, was utilized to determine that for a communication distance of 500 m, the  $\lambda_s$  and  $\lambda_b$  values corresponding to the communication rate of 300 kbps are 33 and 2, and for 150 kbps, they are 64 and 2, respectively. Changes in BER were observed corresponding to the selection of different decision thresholds, as shown in following Figure 8.

It can be observed that at 300 kbps, when the decision threshold is 12, the corresponding BER is  $3.85 \times 10^{-6}$ , and at 150 kbps, when the decision threshold is 19, the corresponding BER is  $4.64 \times 10^{-12}$ . This indicates that as the communication rate changes, the optimal BER and corresponding decision thresholds also change. Lower communication rates result in higher average photon counts, leading to larger corresponding decision

thresholds and lower BERs. Consequently, the impact of LED tailing on communication quality diminishes.

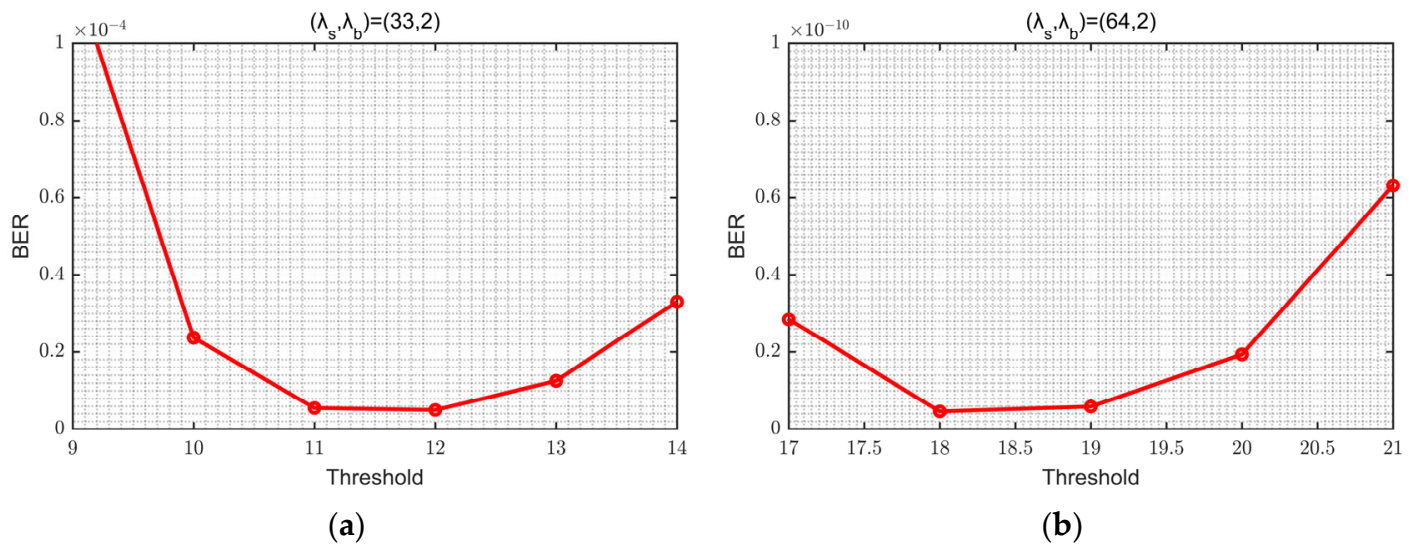


**Figure 8.** (a) The threshold of 300 K communication rate and the change in BER. (b) The threshold of 150 K communication rate and the change in BER.

*3.4. The Relationship between BER and Distance under Different Rates for Both Ideal and Tailing Scenarios*

Simulations were conducted to observe the performance of the BER under different communication rates in both ideal and tailing emission scenarios. The simulation conditions included communication rates of 150 kbps, 200 kbps, and 300 kbps, with the transmitter and receiver elevations set at  $10^\circ$ . The distance varied from 300 m to 900 m to assess the communication quality of the system.

In Figure 9, it can be observed that as the distance increases, the BER gradually rises. Higher communication rates correspond to higher BER, and under the same distance conditions, the BER in the tailing scenario is higher than that in the ideal scenario. It is evident that the impact of LED tailing on communication quality becomes more pronounced with higher communication rates. This phenomenon can be attributed to the following key factors: First, in a UV communication system with constant emission intensity, a higher communication rate under OOK modulation results in a shorter transmission time per bit and, therefore, a decrease in the number of photons emitted per bit. This results in a decrease in the photon decision threshold determined by the maximum likelihood estimation algorithm in UV correlation detection, as shown in Figure 8. When the decision threshold of the maximum likelihood estimation algorithm is low, the impact of the tailing effect on communication quality is more significant. In addition, during the startup and shutdown phases of the LED, a small number of photons will be incorrectly classified as symbol 0 during the reception and decoding process. For a specific LED model and matching circuit, the RC charge and discharge time is fixed, so these misidentified photons will continue to have a fixed impact on the decoding process, as shown in Figure 4, which describes the change in current during the LED emission tailing. At higher communication rates, fewer photons are detected per bit, which will amplify the impact of the LED tailing effect on the system, resulting in an increased impact of erroneous photons on system performance.

In light of these results, we propose an optimization scheme for communication BER based on altering the transmission signal duty cycle.

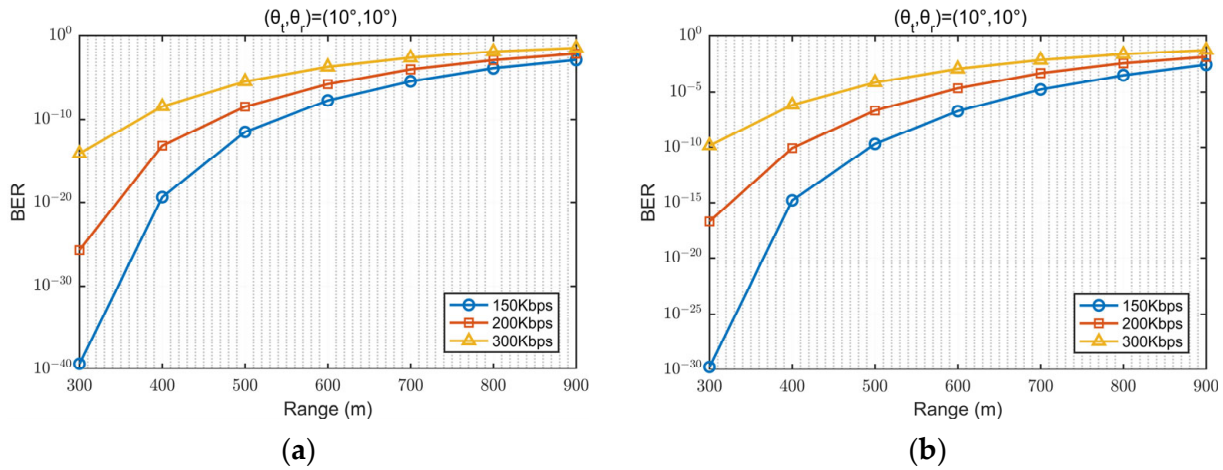


**Figure 9.** (a) The relationship between BER and distance under different rates for ideal scenarios. (b) The relationship between BER and distance under different rates for tailing scenarios.

3.5. The BER Varying with Distance for Different Rates under Different Duty Cycle Conditions

This section conducted three sets of comparative simulations to examine the relationship between BER and distance for different communication rates (300 K, 200 K, and 150 K) under ideal conditions, tailing effects, and varying duty cycles (45%, 47%, and 48%). This was performed to verify whether changing the transmission signal duty cycle could improve communication BER. The simulation results are shown in following Figure 10.

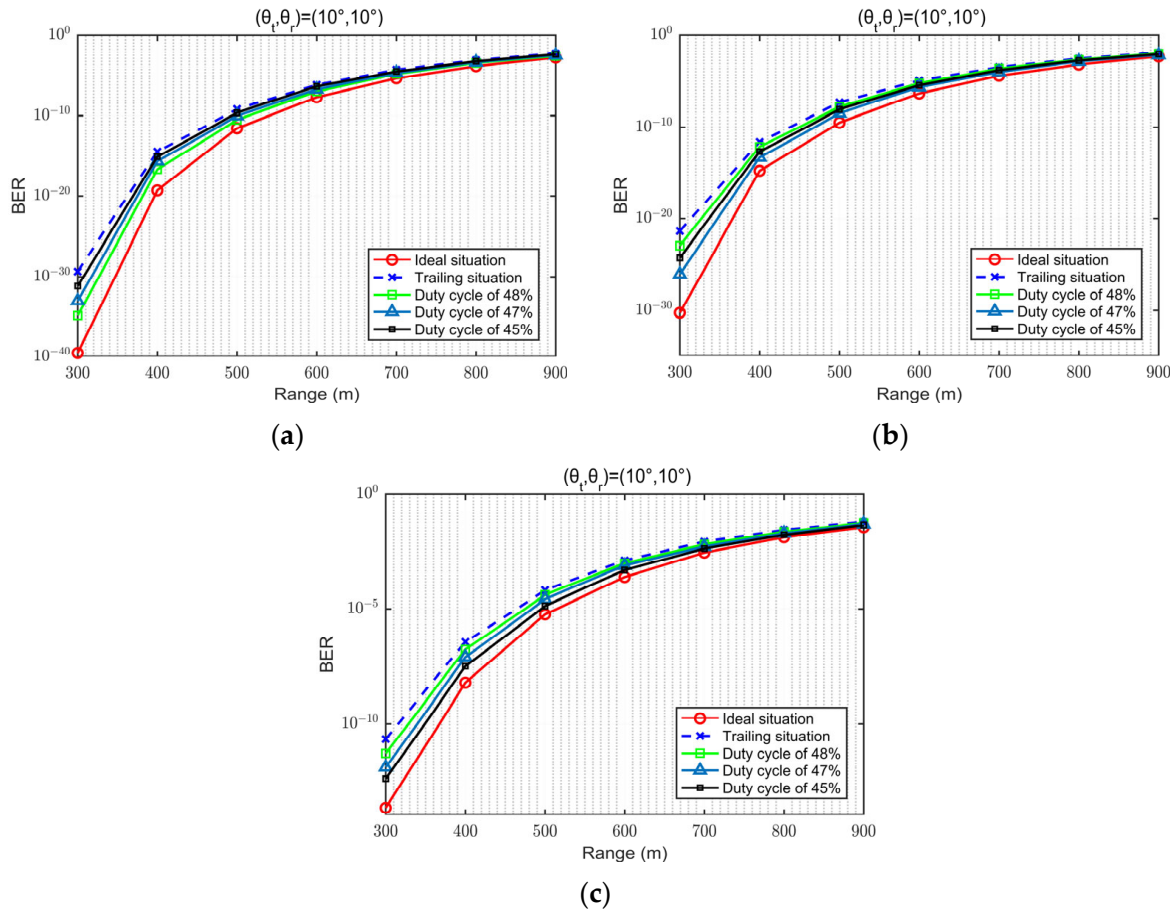


**Figure 10.** (a) The performance of BER at 150 K speed in simulation. (b) The performance of BER at 200 K speed in simulation. (c) The performance of BER at 300 K speed in simulation.

In Figure 10a, it can be observed that, at a rate of 150 K, the BER performances for all three sets of varying duty cycles are superior to the tailing scenario, with 48% being the optimal choice and 45% slightly outperforming tailing. In Figure 10b, for a communication rate of 200 K, 47% is the optimal duty cycle, with 48% and 45% showing similar performance, both better than tailing. In Figure 10c, for a communication rate of 300 K, 45% is the optimal duty cycle, with 48% slightly better than tailing.

The phenomenon where the optimal BER performance corresponds to different duty cycles for different communication rates is attributed to the fact that at higher communication rates, the duration of individual symbols and photon energy is smaller compared to lower rates. However, the duration of LED tailing remains constant regardless of the communication rate change. The pulse width of a 6 k low-speed frame is tens of times larger than that of a 300 k high-speed frame. Therefore, changing the emission duration by the same proportion has a much greater impact on the low-speed frame than on the high-speed frame. Under the same tailing effect, high-speed frames require a lower transmission duty cycle to achieve minimal BER, compensating for the impact. In contrast, low-speed frames, due to their longer per-bit transmission time, are less affected by tailing, requiring only slight adjustments to the duty cycle to achieve minimal BER. When both high-speed and low-speed frames achieve minimal BER, the duty cycle for low-speed frames is closer to the original 50% setting. This indicates that LED emission tailing has a greater impact on high-speed frames than on low-speed frames. To improve communication quality by adjusting the duty cycle, it is necessary to set the duty cycle for low-speed frames closer to the 50% range.

Based on the above simulation results, it is verified that the digital signal processing approach of this scheme can optimize the problem of increased BER of the communication system due to LED tailing under OOK modulation. This also provides guidance for hardware design.

#### 4. Field Experiments

Based on the design system parameters derived from simulation results and the equipment used in Table 1, we conducted outdoor tests to evaluate the system performance. In this system, it is important to note that there is a slight deviation between the wavelength of the ultraviolet light source and the peak wavelength of the optical filter. This deviation is determined by the physical properties of the ultraviolet optical filter, specifically its bandwidth. If we can choose an optical filter that matches the wavelength of the ultraviolet light source, communication performance will be further enhanced.

**Table 1.** Experimental devices and parameter values.

Devices	Parameters	Valus
UV LED	Wavelength	265 nm
	Optical power	100 mW
	Typical luminous Angle	150°
	Radiant Efficiency	typ. 5.7%
UV optical filter	Peak wavelength	262 nm
	Peak transmittance	34%
	Field angle	±5°
PMT	Spectral response	From 160 nm to 320 nm
	Quantum efficiency	20%
	Aperture size	2 cm <sup>2</sup>
ADC	Sampling rate	500 MSPS
	Resolution ratio	12-Bit Resolution
	Input bandwidth	2.3-GHz
	Clock latency	3.5 Clock Cycles
	Aperture size	14 mm × 14 mm

#### 4.1. Prototype and Field Testing Platform Display

To evaluate the real-time communication capability of the ultraviolet communication system under tailing effects and duty cycle variations, we set up a testing platform outdoors and conducted experiments on the BER at different distances. Figure 11a illustrates the relative positions of the transmitter and receiver, while Figure 11b depicts the physical prototype and the constructed outdoor testing platform.

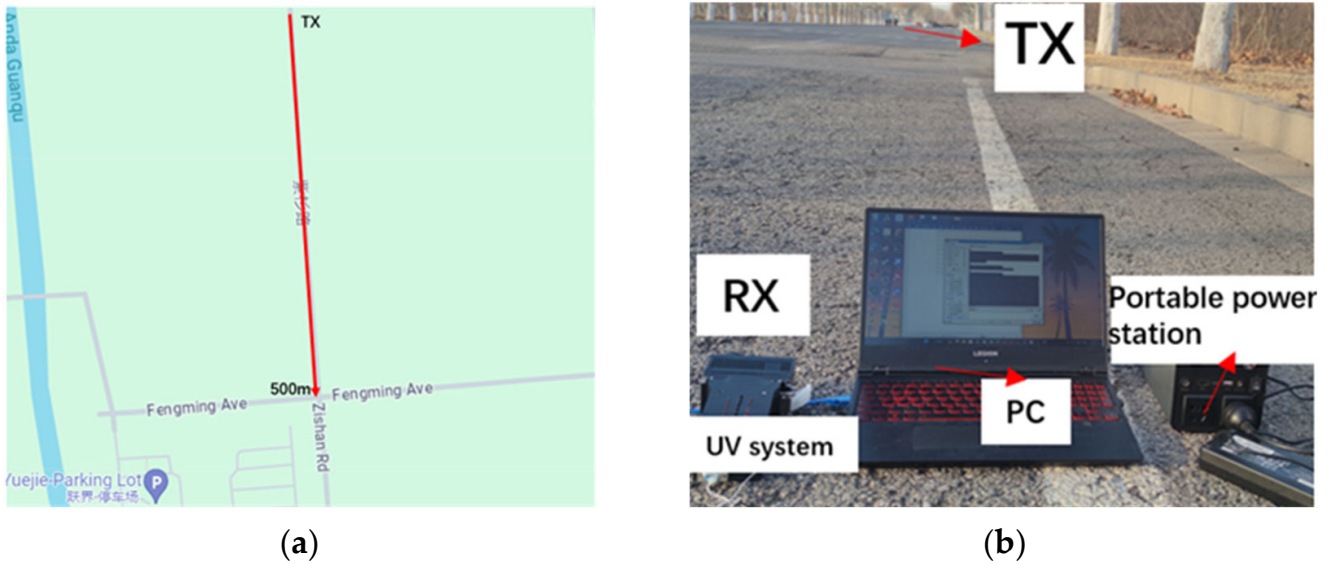


Figure 11. (a) Distance display on map. (b) Physical setup diagram for field experiment.

During the testing, we varied the communication distance from 500 m to 700 m and recorded the performance of BER under different duty cycle settings and tailing effect influences at various distances. The transmitter and receiver were both set at a 10-degree offset angle.

#### 4.2. Testing of Modulation Circuitry and PMT Detection Output Waveforms

In the laboratory, the optoelectronic signals of the transmitter and receiver were tested using an oscilloscope. The communication rate in the test environment was 150 kbps, as depicted in Figure 12.

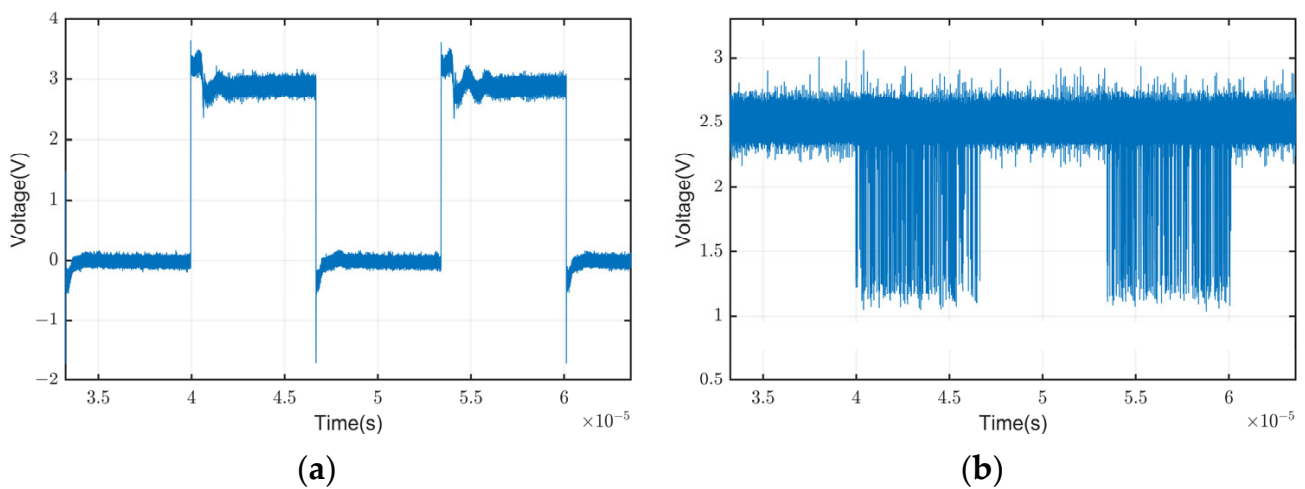
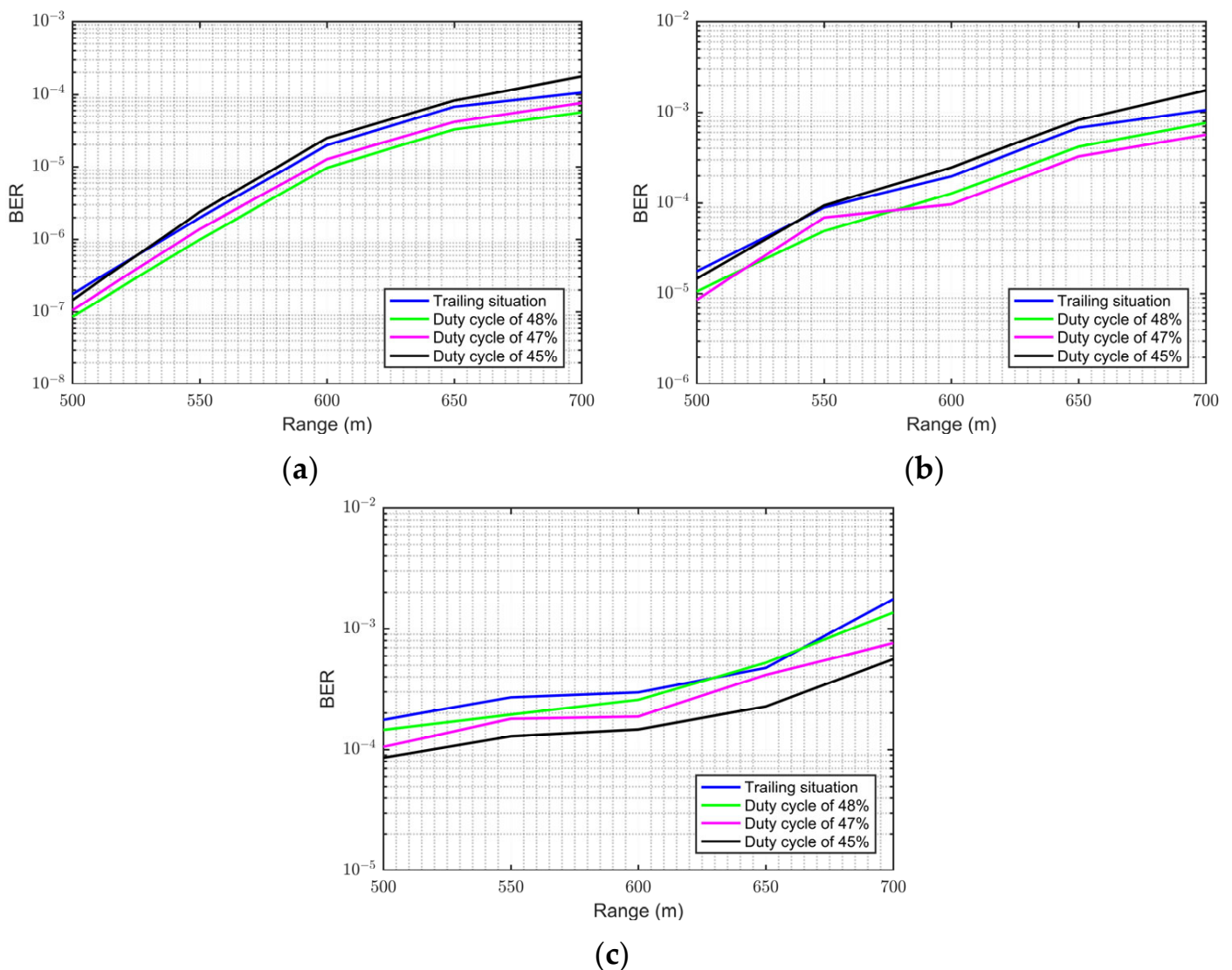


Figure 12. (a) Testing of modulation circuitry output waveforms. (b) Testing of PMT detection output waveforms.

Figure 12a illustrates the waveform signal output from the transmission modulation circuit, while Figure 12b displays the waveform signal of photoelectrons detected by the PMT. Each photoelectron pulse corresponds to one or multiple photoelectrons detected by the PMT. Due to the limited laboratory space, the path loss caused by channel attenuation is relatively low, resulting in a denser detection of photoelectrons by the PMT at this time.

4.3. Analysis of BER Variation with Tailing Effects and Duty Cycle Changes

During outdoor experiments, the straight-line distance between the transmitter and receiver ranged from 500 m to 700 m, with communication tests conducted every 50 m. Simultaneously, for each communication experiment, the system was tested at a rate of 150 kbps under different conditions of tailing effects and duty cycles set at 48%, 47%, and 45%, with the BER results subsequently compiled. Following this, experiments were conducted at rates of 200 kbps and 300 kbps. Figure 13 depicts the curve of BER variation with communication distance in the experimental tests.



**Figure 13.** (a) The performance of BER at 150 K speed. (b) The performance of BER at 200 K speed. (c) The performance of BER at 300 K speed.

It was observed that, compared to the BER data measured under the influence of tailing effects, the BER corresponding to the optimal duty cycle for each communication rate was reduced. This experimental evidence demonstrates that changing the signal duty

cycle can improve the BER increase caused by LED tailing effects in UV communication systems. For a communication rate of 150 kbps, the best BER performance occurred when the transmission signal had a duty cycle of 48%. At 200 kbps, the optimal performance was observed with a 47% duty cycle, although in the range of 520 m to 570 m, the 48% duty cycle performed better. The optimal duty cycle setting for 300 kbps was found to be 45%. However, it is noteworthy that under specific duty cycle conditions, the BER was worse compared to the influence of tailing effects. This is because excessive adjustment of the BER can lead to excessive loss of photons in the intensity of the symbol 1 signal. When the additional BER impact caused by this loss exceeds the BER reduction impact caused by the symbol 0, the BER will further deteriorate.

## 5. Conclusions

In this paper, a novel scheme is proposed for reducing the communication BER by mitigating the tailing effect in LED light sources under OOK modulation. The tailing phenomenon, which is a significant issue affecting the performance of UV links, leading to signal fluctuations at the receiver and thereby increasing the system BER, especially evident during high-speed communication, is considered. The impact of path loss and tailing effects of the light source on the performance of UV communication systems is analyzed, and the probability density functions (PDFs) of signals sent and received ( $\lambda_s$  and  $\lambda_b$ ) are derived. Utilizing these derivations, an analysis of the error phenomena caused by tailing is conducted, and a UV communication scheme is proposed based on adjusting the duty cycle to reduce the BER.

Closed-form expressions for the signal transmission BER are first derived based on a single-scattering model, along with expressions for the Poisson distribution based on the probability of UV photons. Simulation and experimental analyses of the proposed UV system are then conducted based on these expressions. Simulation and experimental results demonstrate that for higher communication rates, the tailing effect significantly impacts the BER, whereas for lower rates, the BER remains relatively insensitive. This is because the tailing effect is determined by the LED response characteristics and manifests as a fixed value over time, with higher communication rates acting on individual symbols for shorter durations, thus resulting in greater tailing effect influence. Further analysis is conducted to determine the optimal duty cycle settings for communication rates sensitive to the tailing effect, concluding that for rates of 150 k, the optimal duty cycle setting is 48%; for 200 k, it is 47%; and for 300 k, it is 45%. For higher communication rates, adopting lower duty cycle settings can notably reduce the BER.

In conclusion, the UV communication scheme proposed in this paper, based on altering the signal duty cycle, holds significant importance in reducing the BER and optimizing system performance. Through experimental and simulation analyses, the effectiveness of this scheme is validated, and practical recommendations are provided for different communication rates, offering valuable insights and guidance for the design and optimization of UV communication systems.

**Author Contributions:** Conceptualization, Y.J. and Y.Z.; methodology, Y.J. and Y.Z.; software, Y.J., Y.Z. and L.K.; validation, Y.J., Y.Z. and R.L.; formal analysis, L.K. and R.L.; writing—original draft preparation, Y.Z.; writing—review and editing, J.N. and Y.J.; project administration, J.L., Y.J. and Y.Z. made equal contributions to this work. All authors have read and agreed to the published version of the manuscript.

**Funding:** This research was funded by the National Natural Science Foundation of China (NSFC), grant number 62231005.

**Institutional Review Board Statement:** Not applicable.

**Informed Consent Statement:** Not applicable.

**Data Availability Statement:** The data are contained within the article.

**Conflicts of Interest:** The authors declare no conflicts of interest.

## References

1. Li, S.; Gong, C.; Xu, Z. Visible light communication performance in weak illumination environment. In Proceedings of the 2015 Opto-Electronics and Communications Conference (OECC), Shanghai, China, 28 June 2015.
2. Hamza, A.S.; Deogun, J.S.; Alexander, D.R. Classification framework for free space optical communication links and systems. *IEEE Commun. Surv.* **2018**, *21*, 1346–1382. [[CrossRef](#)]
3. Shaw, G.A.; Siegel, A.M.; Model, J. Extending the range and performance of non-line-of-sight ultraviolet communication links. In Proceedings of the Unattended Ground, Sea, and Air Sensor Technologies and Applications VIII, Orlando/Kissimmee, FL, USA, 2 May 2006.
4. Xu, Z.; Sadler, B.M. Ultraviolet communications: Potential and state-of-the-art. *IEEE Commun. Mag.* **2008**, *46*, 67–73.
5. Lin, W.Y.; Chen, C.Y.; Lu, H.H.; Chang, C.H.; Lin, Y.P.; Lin, H.C.; Wu, H.W. 10m/500Mbps WDM visible light communication systems. *Opt. Express* **2012**, *20*, 9919–9924. [[CrossRef](#)] [[PubMed](#)]
6. Belov, V.V.; Juwiler, I.; Blaunstein, N.; Tarasenkov, M.V.; Poznakharev, E.S. NLOS communication: Theory and experiments in the atmosphere and underwater. *Atmosphere* **2020**, *11*, 1122. [[CrossRef](#)]
7. Moriarty, D.; Hombs, B. System design of tactical communications with solar blind ultraviolet non line-of-sight systems. In Proceedings of the MILCOM 2009—2009 IEEE Military Communications Conference, Boston, MA, USA, 18 October 2009.
8. Ding, H.; Chen, G.; Majumdar, A.K.; Sadler, B.M.; Xu, Z. Modeling of non-line-of-sight ultraviolet scattering channels for communication. *IEEE J. Sel. Areas Commun.* **2009**, *27*, 1535–1544. [[CrossRef](#)]
9. Xu, Z.; Ding, H.; Sadler, B.M.; Chen, G. Analytical performance study of solar blind non-line-of-sight ultraviolet short-range communication links. *Opt. Lett.* **2008**, *33*, 1860–1862. [[CrossRef](#)] [[PubMed](#)]
10. Wang, L.; Xu, Z.; Sadler, B.M. Non-line-of-sight ultraviolet link loss in noncoplanar geometry. *Opt. Lett.* **2010**, *35*, 1263–1265. [[CrossRef](#)] [[PubMed](#)]
11. Reilly, D.M. Atmospheric Optical Communications in the Middle Ultraviolet. Ph.D. Thesis, Massachusetts Institute of Technology, Cambridge, MA, USA, 1976.
12. Du, A.; Wang, Y.; Zhang, J.; Zou, C.; Xiang, Z.; Liu, J.; Xue, C. Implementation of large angle low error non-line-of-sight ultraviolet communication system. *Opt. Commun.* **2024**, *558*, 130227. [[CrossRef](#)]
13. Borah, D.K.; Mareddy, V.R.; Voelz, D.G. Single and double scattering event analysis for ultraviolet communication channels. *Opt. Express* **2021**, *29*, 5327–5342. [[CrossRef](#)] [[PubMed](#)]
14. Liao, L.; Li, Z.; Lang, T.; Chen, G. UV LED array based NLOS UV turbulence channel modeling and experimental verification. *Opt. Express* **2015**, *23*, 21825–21835. [[CrossRef](#)] [[PubMed](#)]
15. Liao, L.; Drost, R.J.; Li, Z.; Lang, T.; Sadler, B.M.; Chen, G. Long-distance non-line-of-sight ultraviolet communication channel analysis: Experimentation and modelling. *IET Optoelectron.* **2015**, *9*, 223–231. [[CrossRef](#)]
16. Xu, C.; Zhang, H.; Cheng, J. Effects of haze particles and fog droplets on NLOS ultraviolet communication channels. *Opt. Express* **2015**, *23*, 23259–23269. [[CrossRef](#)] [[PubMed](#)]
17. Siegel, A.M.; Shaw, G.A.; Model, J. Short-range communication with ultraviolet LEDs. In Proceedings of the Fourth International Conference on Solid State Lighting, Denver, CO, USA, 20 October 2004.
18. Zuo, Y.; Meng, L.; Li, F.; Wu, J.; Zhang, J.; Zhang, J. Performance Analysis of LDPC in Spatially Multiplexed MIMO UVC System. In Proceedings of the 2018 Asia Communications and Photonics Conference (ACP), Hangzhou, China, 26–29 October 2018.
19. Wang, K.; Gong, C.; Zou, D.; Jin, X.; Xu, Z. Demonstration of a 400 kbps real-time non-line-of-sight laser-based ultraviolet communication system over 500 m. *Chin. Opt. Lett.* **2017**, *15*, 040602. [[CrossRef](#)]
20. Luetgten, M.R.; Shapiro, J.H.; Reilly, D.M. Non-line-of-sight single-scatter propagation model. *JOSA A* **1991**, *8*, 1964–1972. [[CrossRef](#)]

**Disclaimer/Publisher’s Note:** The statements, opinions and data contained in all publications are solely those of the individual author(s) and contributor(s) and not of MDPI and/or the editor(s). MDPI and/or the editor(s) disclaim responsibility for any injury to people or property resulting from any ideas, methods, instructions or products referred to in the content.